Letter

Pump-induced magnon anticrossing due to three-magnon splitting and confluence

Tao Qu,[1,*] Yuzan Xiong,[1] Xufeng Zhang,[2,3] Yi Li,[4] and Wei Zhang[1,†]

[1]*Department of Physics and Astronomy, University of North Carolina at Chapel Hill, Chapel Hill, North Carolina 27599, USA*

[2]*Department of Electrical and Computer Engineering, Northeastern University, Boston, Massachusetts 02115, USA*

[3]*Department of Physics, Northeastern University, Boston, Massachusetts 02115, USA*

[4]*Materials Science Division, Argonne National Laboratory, Argonne, Illinois 60439, USA*

(Received 5 August 2024; revised 23 April 2025; accepted 7 May 2025; published 23 May 2025)

We present a plausible mechanism for achieving a magnon-magnon level repulsion spectrum originating from the oscillation between the splitting and confluence in a three-magnon scattering process. When a magnetostatic mode on a YIG sphere is pumped by a microwave signal near the magnon resonance frequency with an increasing amplitude, the generated magnon condensate at half of the pumping frequency exerts a backaction to the original magnon mode. Such a strong nonlinear coupling manifests a striking feature of a "bending effect" of the magnetostatic mode spectra, akin to the anticrossing observed in a strongly coupled magnon-photon system.

DOI: 10.1103/PhysRevB.111.L180410

Introduction. Hybrid magnonics is an emerging interdisciplinary field that explores coherent interactions of magnons with other types of excitations such as photons, phonons, spins, and magnons themselves [1–3]. The mode hybridization is usually achieved by a strong coupling of magnons with another resonant mode, manifesting a mode anticrossing in the frequency spectrum [4–10]. The capability of maintaining phase coherence has led to the realization of many novel and interesting physical phenomena with magnons, such as level attraction [11], nonreciprocity [12,13], exceptional points [14,15], and Floquet engineering [16]. They benefit from the high controllability of the magnon system, including frequency tunability with magnetic field and coupling control by changing the spatial location [17]. These phenomena open opportunities in magnon-based coherent information processing and offer new potentials in quantum magnonics [18–21].

One unique property of magnons is their nonlinearity, which is at the heart of magnonics from both the fundamental understanding and the technological leverage [22,23]. When the population of a magnon eigenmode is excited above a threshold value, the mode will start to overlap with other eigenmodes, leading to a finite coupling due to magnetic dipolar and exchange interactions [24–27]. This amplitude-dependent nonlinear coupling leads to energy redistribution among different magnon eigenmodes by three-magnon or four-magnon scattering [28–31], which is referred to as the Suhl instability [32]. The process usually results in additional energy loss and decoherence of the system. A controlled and coherent energy redistribution process has rarely been explored for coherent addressing of magnons. The only exception to date is the Bose-Einstein condensation of magnons [33–36]. However, creating a coherent magnon condensate requires the magnon thermalization to be faster than the magnon relaxation, thus limiting the application in low-amplitude, coherent magnon engineering.

Recently, an interesting finding of a pump-induced magnon mode suggests that the nonlinear magnon interaction can be harnessed for controlling coherent energy transduction [37–39]. Using a strong microwave pump, the excited magnetostatic (MS) magnon mode manifests an anticrossing feature, in which the pump power controls the level splitting. However, the microscopic origin of such a process is yet unexplored, limiting the further engineering of such a phenomenon for coherent magnon control.

In this work, we show that this pump-induced magnon anticrossing is due to the coupling between the MS mode and the magnon condensate via a coherent three-magnon splitting and confluence process [28,40]. Using a comprehensive analytical model, we show that the coupling strength is proportional to the population of the magnon condensate that is generated via the nonlinear magnon scattering, in which the power threshold for observing the magnon anticrossing matches well with the power threshold of a single-tone, nonlinear magnon broadening. In addition, we reveal that a cutoff frequency exists for the pump-induced magnon anticrossing for each MS mode including the high-order ones. The cutoff frequency is closely linked to the selection rule of three-magnon scattering: above the cutoff frequency, there is no available magnon mode due to the required energy conservation, and the three-magnon scattering is therefore forbidden. Our results open up additional avenues for coherent magnon interaction with nonlinear magnonic processes.

Experiments. Our experimental setup is illustrated in Fig. 1(a): A YIG sphere with a diameter of 1.0 mm is placed on top of the signal line of a coplanar waveguide (CPW). The external magnetic field, H, is applied in-plane (xy) and along the signal line, corresponding to the perpendicular excitation geometry ($H \perp h_{\mathrm{rf}}$). The system response is monitored by a weak microwave probe signal when a strong microwave pump (f_d)

*Contact author: qutao@unc.edu

†Contact author: zhwei@unc.edu

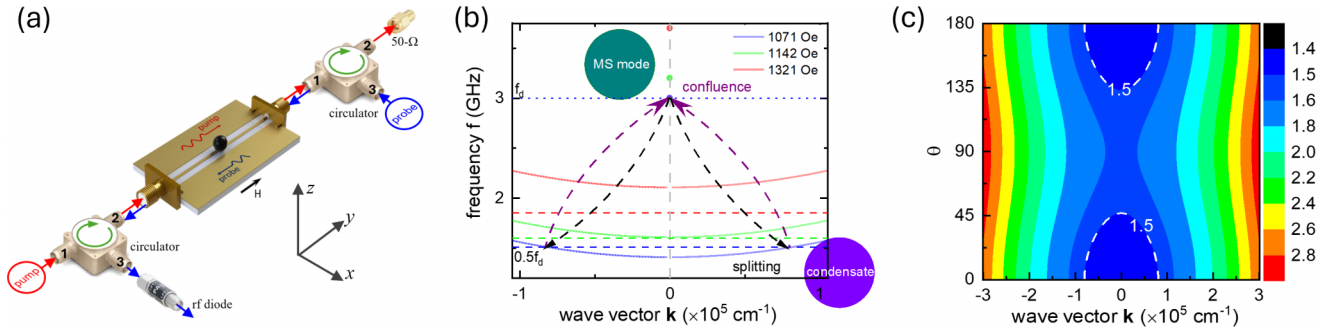

FIG. 1. (a) Schematics of the experimental setup. The counterpropagating (enabled by a pair of broadband circulator) pump and probe signals interact with the YIG sphere on the CPW. The spin wave excitations are detected by field-modulation FMR using a microwave diode and a lock-in amplifier. The magnetic field H is applied along the signal line, satisfying the perpendicular excitation and pumping geometry. (b) Illustration of the three-magnon splitting and confluence, forming a "Rabi-like" process giving rise to coherent coupling between the condensate state and the magnetostatic mode and the avoided level repulsion. Three representative magnon dispersions are exemplified taking the first magnetostatic mode $m = 1$: $H = 1071.0$ Oe (blue), 1142 Oe (green), and 1321 Oe (red), corresponding to different pump frequencies, $f_d = 3.0$ GHz, 3.2 GHz, and 3.7 GHz, respectively. Above the frequency threshold of the three-magnon scattering (red), the requirement of magnon frequency of $\frac{1}{2}f_d$ is not satisfied for the magnon wave vector $\mathbf{k} \neq 0$. (c) The color map of the intrinsic frequency f of the magnon in the spherical axes of the wave vector amplitude and the polar angle θ. The intrinsic frequency is degenerate in the azimuthal angle ϕ, thus not illustrated. The intrinsic frequency at $\frac{f_d}{2} = 1.5$ GHz is plotted in the egg-shaped contour line (white dashed line) corresponding to the multiple degenerate $\mathbf{k} \neq 0$ modes ($|\mathbf{k}|, \theta, \phi$), an extension to (b) with magnetostatic frequency f_d=3.0 GHz in the blue line.

is applied, which induces the magnon condensate through perpendicular pumping; see Fig. 1(b). This condensate is different from the Bose-Einstein condensate [33] in parametric pumping: a microwave photon creating two primary magnons and thermal relaxation of primary magnons to a quasiequilibrium distribution of thermalized magnons in four-magnon scattering. The magnetostatic mode and the condensate mode dominate our system, shown in Fig. 2(b), while the three-magnon scattering involving both splitting and confluence occurs solely between these dominant magnons, introducing the intensity of the dominant modes far deviating from their thermal level. Thus, this system is not in quasiequilibrium and the chemical potential is not adopted to describe this Rabi-like system. Multiple MS modes are present in our experiment, as will be discussed later.

The pump and probe signals propagate in opposite directions in the CPW by using a pair of broadband circulators at each end of the CPW. The pump path is terminated with a 50-Ω resistor to eliminate reflection. The probe signal transmitted through the device is sent to a microwave diode and

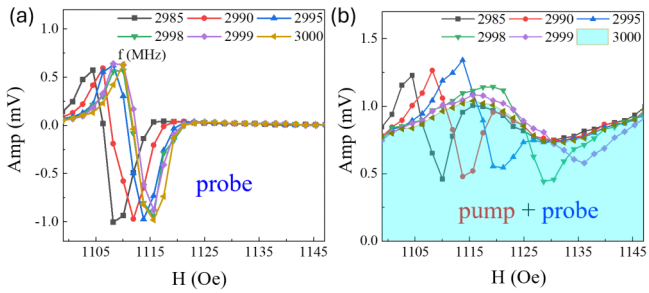

FIG. 2. (a), (b) The first magnetostatic mode, $m = 1$ (centered around $H = 1115.0$ Oe), measured at different frequencies in the situation where a pump ($f_d = 3.0$ GHz) is off (a), or on (b). MS: magnetostatic.

detected by a lock-in amplifier using the field-modulation ferromagnetic resonance (FMR) technique [41], where a reference signal from the lock-in amplifier is amplified and fed to a modulation coil and modulates the external field with the reference frequency. The microwave diode signal is lock-in amplified at this frequency. The output of the lock-in amplifier is then proportional to the field derivative of the transmitted microwave power [42].

Results and discussion. In our system, the three-magnon splitting and confluence take place under the strong microwave pump; see Fig. 1(b). Each MS mode excited at f_d splits into a pair of magnons in the spin wave modes at the half frequencies $f_d/2$ with opposite wave vectors, and they recombine to form an f_d mode following an oscillating fashion, akin to a "Rabi-like" oscillation in strongly coupled systems. For a lower frequency of MS mode, the magnon dispersion satisfies $f_d/2$ at specific wave vectors. Upon increasing the frequency of the MS mode through enhancing the corresponding resonance magnetic field based on the Kittel equation, such condition breaks at a threshold frequency where only a pair of opposite wave vectors meet the frequency requirement of $f_d/2$. Above this frequency threshold, three-magnon scattering is disabled fundamentally due to no wave vector in the magnon dispersion satisfying the frequency $f_d/2$. The Hamiltonian of such splitting and confluence process can be described as

$$H_{3m} = \tfrac{1}{2}\Sigma_k(\zeta_{\mathbf{k}} c_0 c^*_{\mathbf{k}} c^*_{-\mathbf{k}} + \zeta^*_{\mathbf{k}} c^*_0 c_{\mathbf{k}} c_{-\mathbf{k}}), \quad (1)$$

where c_0 denotes the wave vector $\mathbf{k} = 0$ MS spin waves, c_k the parametrically generated $\mathbf{k} \neq 0$ spin waves (which eventually form the magnon condensate), and $\zeta_{\mathbf{k}} = \hbar\gamma M_s \sin(2\theta)/4$ is the three-magnon coupling coefficient, where $\hbar$ is the reduced Planck constant, γ is the gyromagnetic ratio, M_s is the magnetization saturation, and θ is the angle between the wave vector $\mathbf{k}$ and the applied magnetic field; thus the maximum coupling occurs at $\theta = 45^\circ$ when fulfilling the conditions of three-

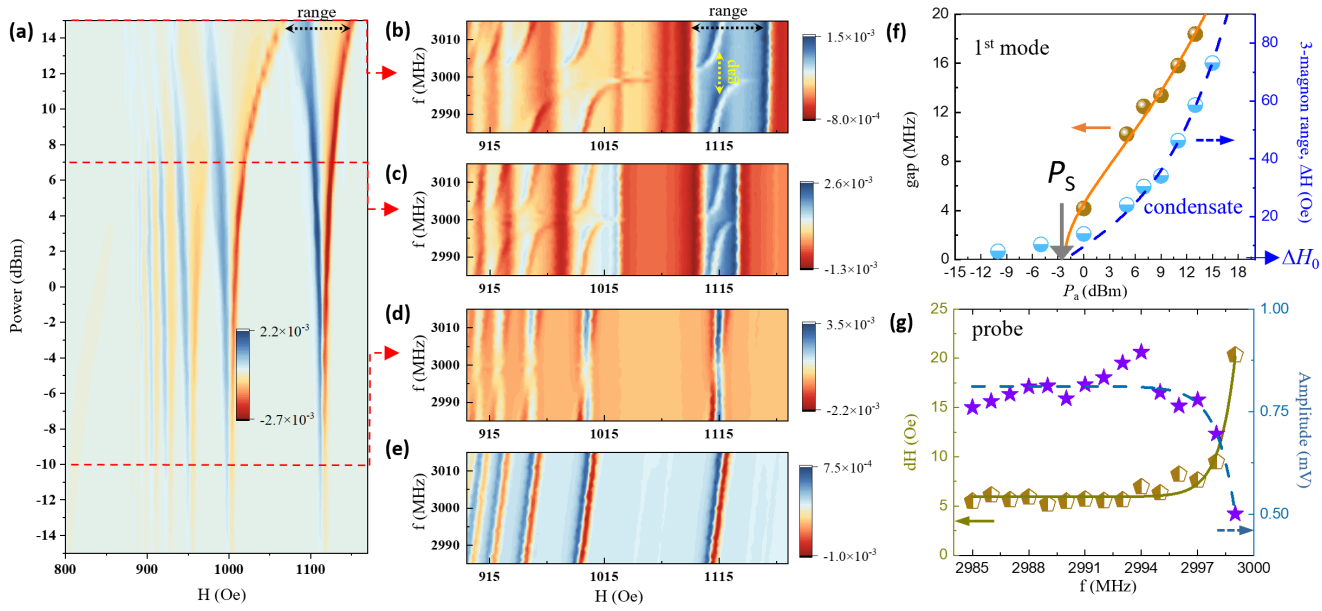

FIG. 3. (a) Magnon spectra measured at 3.0 GHz at different input microwave power and at a broad magnetic-field range covering at least six identifiable MS modes. (b)–(e) The f-H dispersion spectra scanned near the pump frequency ($f_d = 3.0$ GHz) and at selective input power levels (b) 15 dBm, (c) 7 dBm, (d) −10 dBm, and (e) no pump. (f) The extracted anticrossing "gap" and condensate "range" versus the input power for the 1st MS mode. A gap cannot be clearly identified for powers below 0 dBm. Lines are theoretical fits. (g) The frequency-dependent linewidth and signal amplitude of the 1st MS mode in response to a 15 dBm pump at 3.0 GHz.

magnon scattering. Simultaneously, $\zeta_{\mathbf{k}}$ is a real number in the sphere system, where $\zeta_{\mathbf{k}}^* = \zeta_{\mathbf{k}}$. Note that the three-magnon dispersion of the YIG sphere is slightly different from that of the YIG film [28,30]. The color map of the intrinsic frequency f of the magnon in the spherical axes of the wave vector amplitude and the polar angle θ is illustrated in Fig. 1(c). More details on this theoretical aspect are included in the Supplemental Material [43] (see also Refs. [44–48] therein).

When the pump is weak, the magnon splitting and accordingly the intensity of the induced condensate are insignificant. However, as the pump amplitude increases, two emergent observations arise: (i) The magnon spectra broaden significantly with much suppressed susceptibility due to the onset of the three-magnon scattering [49], and (ii) the confluence (accordingly, the backaction to the MS magnon mode) becomes prominent and effectively introduces an additional damping channel to the MS mode.

As an example, Figs. 2(a) and 2(b) show the fundamental MS mode (centered around $H = 1115.0$ Oe) measured at different frequencies in the situation where a pump ($f_d = 3.0$ GHz) is either off (a) or on (b). Due to the field-modulation FMR technique and lock-in detection, the susceptibility of the whole system can be captured. When the pump is off, the signals at different frequencies correspond to the MS mode and are of similar amplitude with no amplitude offset with respect to zero. But, once the pump kicks in, the signal (at the same selected frequencies) is superimposed on a broad plateau, i.e., the continuous spin wave band due to the onset of the three-magnon scattering. In addition, as the MS mode gets near to the pump frequency (3.0 GHz), its amplitude decreases and the line shape broadens, caused by the additional damping channel by its nonlinear coupling to the magnon condensate.

The same effect takes place for multiple MS modes, which can be measured by expanding the sweeping range of the bias magnetic field, as shown in Fig. 3. These modes are identified as the MS modes with mode order $(m, m, 0)$, where $m = 1, 2, 3, \ldots$ is the angular mode number, and the fundamental mode ($m = 1$) corresponds to the FMR mode. The evolution from a common MS mode to a condensate state by the pumping power is well exemplified by the two-dimensional (2D) contour plot in Fig. 3(a), measured at 3.0 GHz: at lower power level (below −2 dBm), individual, sharp resonances with narrow linewidths can be identified, which correspond to the genuine MS modes. However, as the power further increases, the three-magnon process becomes significant with much broadened linewidths and suppressed resonance amplitudes. From Fig. 1(b) it is clear that the possible wave vectors of the scattered magnons are not discrete, but instead they can take a range of values within a broad spin wave continuum. Therefore, the scattered magnons form a continuous spin wave band (the condensate), whose field span (range, ΔH) can be measured and characterized directly from the 2D contour plot.

The level of formation of such condensate has a direct impact on the MS mode by its backaction: Figures 3(b)–3(e) show the f-H relation contour plots measured (using a −10 dBm probe) at a fixed pump of $f_d = 3.0$ GHz and at selective power levels. When the pump is absent, Fig. 3(e), linear dispersion of the MS modes is observed. When a small pump is applied (−10 dBm), Fig. 3(d), the backaction of the condensate to the MS mode emerges: One can observe both a finite spin wave band (the "range") and the MS modes, but they are almost only linearly overlapped (weakly coupled). As power further increases, Figs. 3(c) and 3(b), first, the "range" further expands, and second, the backaction of the condensate to the

MS mode becomes prominent, resulting in the "bending" of the MS mode spectra, akin to an anticrossing "gap" centered around the pump (f_d). Notably, such a "bending effect" only lives up to the extent confined by the condensate "range" and sharply cuts off at the boundary. This is in stark contrast with a conventional anticrossing feature observed for common hybrid photon-magnon systems, where such bounds do not exist for a conventional anticrossing feature.

We develop a semianalytical model to accurately describe the nonlinear dynamics of magnon scattering through the equation of motion, which is derived from a 1st-order Hamiltonian including the self-energy of the magnons, and the scattering between the MS ($\mathbf{k} = 0$) and spin wave ($\mathbf{k} \neq 0$) magnons. The scattering process includes both the forward creation process, i.e., the annihilation of one MS magnon with the creation of two spin wave magnons, and its inverse effect, the backward confluence process, i.e., the creation of one MS magnon with the annihilation of two spin wave magnons. The scattering occurs at a long timescale, e.g., submicrosecond, compared to the short timescale of the magnetization precession in magnons, e.g., subnanosecond. The scattering process can be described by the dynamic equations [40]

$$\dot{c}_0 = -\eta_0 c_0 - \zeta_{\mathbf{k}} c_{\mathbf{k}}^2 + \upsilon h_a, \tag{2}$$

$$\dot{c_{\mathbf{k}}} = -\eta_k c_{\mathbf{k}} + \zeta_{\mathbf{k}} c_0 c_k, \tag{3}$$

where c_0 ($c_{\mathbf{k}}$) and η_0 (η_k) are the intensity and relaxation rate of the MS (spin wave) magnons, respectively. $\zeta_{\mathbf{k}}$ is the exchange strength between MS and spin wave magnon modes. υ is the capability of the driving force h_a, of the microwave field to create $\mathbf{k} = 0$ magnons, where the force $h_a = \sqrt{\frac{2P_a}{R_{\text{load}}}}/d_{\text{CPW}}$ is determined by the microwave power P_a, the load resistance R_{load}, and the width of the coplanar waveguide d_{CPW}.

The constraints for these wave vectors $\mathbf{k}$ follow the laws of energy ($f_{\mathbf{k}} + f_{-\mathbf{k}} = f_{\mathbf{k}=0}$) and momentum conservation: The magnon pair of $\pm\mathbf{k}$ are created or annihilated spontaneously. The initial condition of the dynamic equations is the intensity of the thermal magnons, where their levels follow the Bose-Einstein distribution $\sim e^{-\hbar\omega_{\mathbf{k}}/k_B T}$, where k_B is the Boltzmann constant and T is the temperature.

The fixed point for the linear regime corresponds to

$$c_0 = \upsilon h_a/\eta_0, \tag{4}$$

$$c_{\mathbf{k}} = 0. \tag{5}$$

In the linear regime, only $\mathbf{k} = 0$ is present and the magnetization undergoes uniform precession. Thus the intensity c_0 in the linear regime is proportional to the microwave driving force h_a. This force is insufficient in amplitude to excite the three-magnon scattering, where $c_{\mathbf{k}} = 0$ until this force enhances to the threshold $h_S = \eta_0\eta_{\mathbf{k}}/(\zeta_{\mathbf{k}}\upsilon)$, i.e., reaching the Suhl instability. Above this threshold, the magnon scattering is triggered and a pronounced $c_{\mathbf{k}}$ is activated.

Mathematically, the nonlinear regime's fixed point yields the magnon intensity c_0 and $c_{\mathbf{k}}$,

$$c_0 = \eta_{\mathbf{k}}/\zeta_{\mathbf{k}}, \tag{6}$$

$$c_{\mathbf{k}} = \sqrt{\frac{\upsilon h_a - \eta_0\eta_k/\zeta_{\mathbf{k}}}{\zeta_{\mathbf{k}}}}. \tag{7}$$

Expressing the spin wave magnon intensity in Eq. (7) within the threshold h_S yields

$$c_{\mathbf{k}} = \sqrt{\frac{\upsilon}{\zeta_{\mathbf{k}}}(h_a - h_S)} \sim \sqrt{\sqrt{P_a} - \sqrt{P_S}}. \tag{8}$$

In the nonlinear regime, the spin wave magnon presents a significant amount, much larger than its original thermal level, due to the three-magnon scattering. Thus this amount reflects the power-tuned coupling between MS and spin wave magnons, and experimentally fingerprints the gap size in Fig. 3(f), where the fit yields a threshold power $P_S = 0.6$ mW (-2.2 dBm). Correspondingly, the three-magnon (condensate) linewidth (range, ΔH), denoted as $\Delta H = 2\Delta\omega_0/\gamma = 2\Delta H_0\sqrt{P_a/P_S - 1}$, is shown and fitted in Fig. 3(f), yielding a generic magnon linewidth $\Delta H_0 = 5.71$ Oe.

Reciprocally, the backaction induces additional damping of the MS mode and attenuation of its amplitude, which are both confirmed in the experiment and summarized in Fig. 3(g), as an example of the 1st MS mode: The peak-to-peak linewidth (δH) increases and the signal amplitude decreases both rapidly as the MS mode frequency is closer to the pump.

Finally, additional strong evidence to our proposed mechanism comes from the concurrent frequency cutoff for both the anticrossing gap and the nonlinear broadening. Because the principles demonstrated above also apply to high-order MS modes ($m > 1$) which are observed in our experiment, we can examine their distinct frequency thresholds for activating such a nonlinear coupling. According to the theory of three-magnon scattering [30,32,40,49], above a certain frequency threshold, the three-magnon process will be prohibited due to absence of magnon bands at the half frequency, illustrated in Fig. 1(b). In order to determine the threshold frequency for each MS mode, comprehensive power spectra were obtained at frequencies between 3.0 to 4.7 GHz at a step of 0.1 GHz (see the Supplemental Material [43]). The threshold frequency for invoking the three-magnon process is determined as 3.6 GHz (1st),4.2 GHz (2nd), 4.4 GHz (3rd), 4.6 GHz (4th), and 4.7 GHz (5th). Figures 4(a)–4(d) show the power scan contour plot at selective frequencies, (a) 4.0, (b) 4.2, (c) 4.5, and (d) 4.7 GHz. It is obvious that as the frequency increases, the magnon bands ("ranges") for each mode progressively disappear (starting from the 1st), after passing the respective threshold frequencies. This leads to a direct voiding of the corresponding "bending effect," revealed by the *f-H* relation measured near the cutoff frequency, in Figs. 4(e)–4(h): The anticrossing "gap" progressively disappears after reaching the cutoff frequencies. Such an observation corroborates the strong correlation between the anticrossing "gap" and the condensate formation via three-magnon splitting and confluence.

Summary. In summary, we report an additional type of nonlinear coupling between a magnon condensate and magnetostatic modes in a YIG sphere, activated by the energy pumping from a waveguide. We show that the magnon condensate can be excited via the nonlinear three-magnon splitting processes, and its backaction to the magnetostatic mode via the confluence process is significantly enhanced

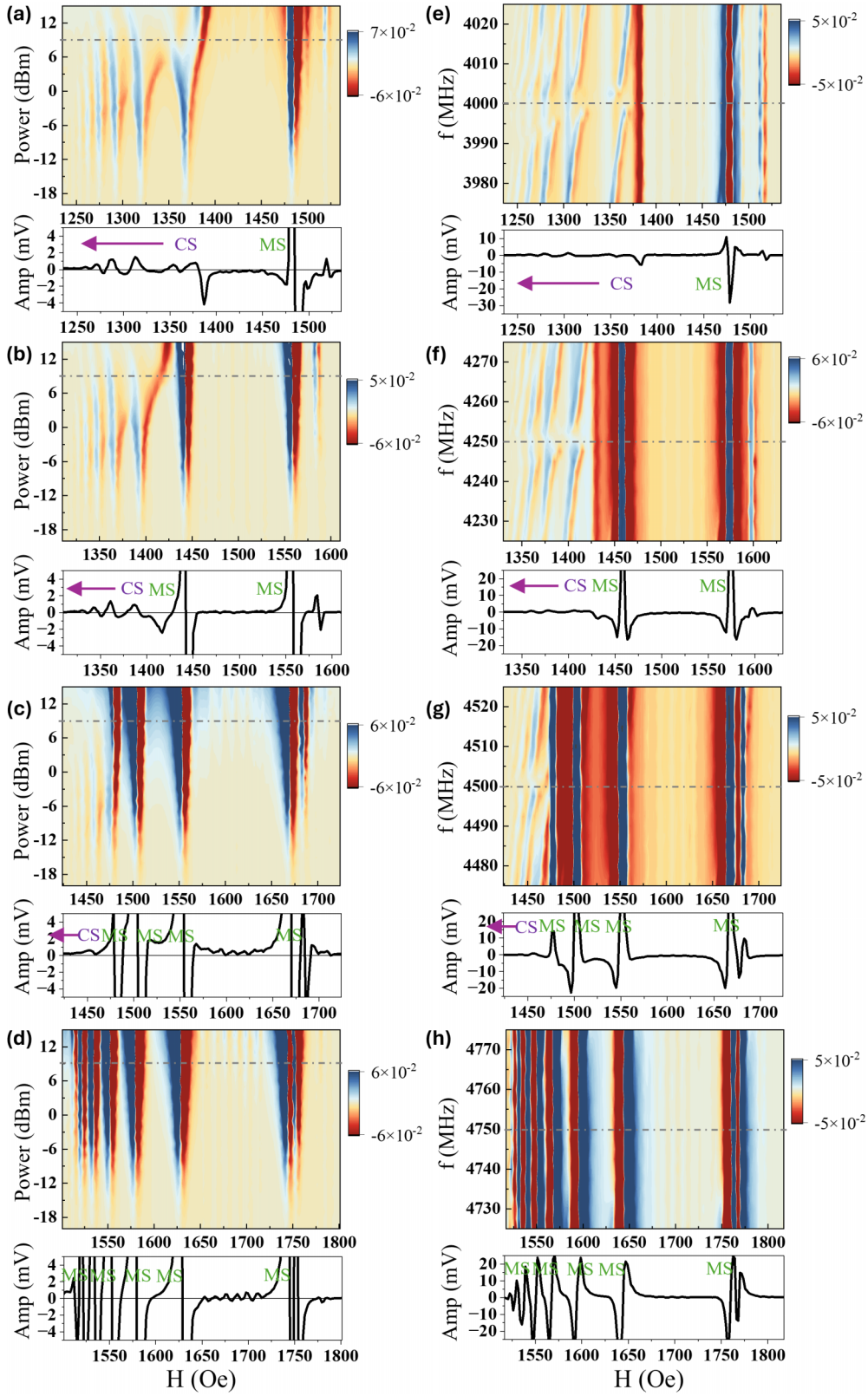

FIG. 4. (a)–(d) Power scan contour plots at selective frequencies: (a) 4.0, (b) 4.2, (c) 4.5, (d) 4.7 GHz. A line-scan trace at a pump power of 9 dBm is shown for each contour plot. MS: magnetostatic mode. CS: condensate mode. The MS and CS modes are identified for each plot. (e)–(h) *f-H* dispersion contour plots measured at a fixed pump power (9 dBm) and at selective frequencies: (e) 4.0, (f) 4.25, (g) 4.5, (h) 4.75 GHz. A line-scan trace at the pump frequency (center of anticrossing gap) is shown for each contour plot.

by the presence of a strong pump signal, which leads to a "bending effect" of the MS mode spectra, akin to an anticrossing "gap" in the strongly coupled magnonic systems. Our mechanism opens another direction for developing engineerable magnonic systems leveraging coupled spin wave phenomena.

Acknowledgments. We thank Vasyl Tyberkevych and Andrei Slavin for valuable discussions about the mechanism of three-magnon scattering. The experimental measurements about pump-induced magnon anticrossing performed at the University of North Carolina at Chapel Hill are supported by the U.S. National Science Foundation (NSF) under Grant No. ECCS-2246254. X.Z. acknowledges support from the NSF (Grant No. ECCS-2337713) and the Office of Naval Research Young Investigator Program (Grant No. N00014-23-1-2144). Y.L. acknowledges support from the U.S. DOE, Office of Science, Basic Energy Sciences, Materials Sciences and Engineering Division, under Contract No. DE-SC0022060.

[1] D. Lachance-Quirion, Y. Tabuchi, A. Gloppe, K. Usami, and Y. Nakamura, Hybrid quantum systems based on magnonics, Appl. Phys. Express **12**, 070101 (2019).

[2] Y. Li, W. Zhang, V. Tyberkevych, W.-K. Kwok, A. Hoffmann, and V. Novosad, Hybrid magnonics: Physics, circuits and applications for coherent information processing, J. Appl. Phys. **128**, 130902 (2020).

[3] D. D. Awschalom, C. R. Du, R. He, F. J. Heremans, A. Hoffmann, J. Hou, H. Kurebayashi, Y. Li, L. Liu, V. Novosad, J. Sklenar, S. E. Sullivan, D. Sun, H. Tang, V. Tyberkevych, C. Trevillian, A. W. Tsen, L. R. Weiss, W. Zhang, X. Zhang *et al.*, Quantum engineering with hybrid magnonic systems and materials (invited paper), IEEE Trans. Quantum Eng. **2**, 1 (2021).

[4] H. Huebl, C. W. Zollitsch, J. Lotze, F. Hocke, M. Greifenstein, A. Marx, R. Gross, and S. T. B. Goennenwein, High cooperativity in coupled microwave resonator ferrimagnetic insulator hybrids, Phys. Rev. Lett. **111**, 127003 (2013).

[5] Y. Tabuchi, S. Ishino, T. Ishikawa, R. Yamazaki, K. Usami, and Y. Nakamura, Hybridizing ferromagnetic magnons and microwave photons in the quantum limit, Phys. Rev. Lett. **113**, 083603 (2014).

[6] X. Zhang, C.-L. Zou, L. Jiang, and H. X. Tang, Strongly coupled magnons and cavity microwave photons, Phys. Rev. Lett. **113**, 156401 (2014).

[7] M. Goryachev, W. G. Farr, D. L. Creedon, Y. Fan, M. Kostylev, and M. E. Tobar, High-cooperativity cavity QED with magnons at microwave frequencies, Phys. Rev. Appl. **2**, 054002 (2014).

[8] L. Bai, M. Harder, Y. P. Chen, X. Fan, J. Q. Xiao, and C.-M. Hu, Spin pumping in electrodynamically coupled magnon-photon systems, Phys. Rev. Lett. **114**, 227201 (2015).

[9] Y. Li, T. Polakovic, Y.-L. Wang, J. Xu, S. Lendinez, Z. Zhang, J. Ding, T. Khaire, H. Saglam, R. Divan, J. Pearson, W.-K. Kwok, Z. Xiao, V. Novosad, A. Hoffmann, and W. Zhang, Strong coupling between magnons and microwave photons in on-chip ferromagnet-superconductor thin-film devices, Phys. Rev. Lett. **123**, 107701 (2019).

[10] J. T. Hou and L. Liu, Strong coupling between microwave photons and nanomagnet magnons, Phys. Rev. Lett. **123**, 107702 (2019).

[11] M. Harder, Y. Yang, B. M. Yao, C. H. Yu, J. W. Rao, Y. S. Gui, R. L. Stamps, and C.-M. Hu, Level attraction due to dissipative magnon-photon coupling, Phys. Rev. Lett. **121**, 137203 (2018).

[12] Y.-P. Wang, J. W. Rao, Y. Yang, P.-C. Xu, Y. S. Gui, B. M. Yao, J. Q. You, and C.-M. Hu, Nonreciprocity and unidirectional invisibility in cavity magnonics, Phys. Rev. Lett. **123**, 127202 (2019).

[13] X. Zhang, A. Galda, X. Han, D. Jin, and V. M. Vinokur, Broadband nonreciprocity enabled by strong coupling of magnons and microwave photons, Phys. Rev. Appl. **13**, 044039 (2020).

[14] D. Zhang, X.-Q. Luo, Y.-P. Wang, T.-F. Li, and J. Q. You, Observation of the exceptional point in cavity magnon-polaritons, Nat. Commun. **8**, 1368 (2017).

[15] X. Zhang, K. Ding, X. Zhou, J. Xu, and D. Jin, Experimental observation of an exceptional surface in synthetic dimensions with magnon polaritons, Phys. Rev. Lett. **123**, 237202 (2019).

[16] J. Xu, C. Zhong, X. Han, D. Jin, L. Jiang, and X. Zhang, Floquet cavity electromagnonics, Phys. Rev. Lett. **125**, 237201 (2020).

[17] Y. Xiong, A. Christy, Y. Dong, A. H. Comstock, D. Sun, Y. Li, J. F. Cahoon, B. Yang, and W. Zhang, Combinatorial split-ring and spiral metaresonator for efficient magnon-photon coupling, Phys. Rev. Appl. **21**, 034034 (2024).

[18] D. Lachance-Quirion, S. P. Wolski, Y. Tabuchi, S. Kono, K. Usami, and Y. Nakamura, Entanglement-based single-shot detection of a single magnon with a superconducting qubit, Science **367**, 425 (2020).

[19] D. Xu, X.-K. Gu, H.-K. Li, Y.-C. Weng, Y.-P. Wang, J. Li, H. Wang, S.-Y. Zhu, and J. Q. You, Quantum control of a single magnon in a macroscopic spin system, Phys. Rev. Lett. **130**, 193603 (2023).

[20] H. Y. Yuan, Y. Cao, A. Kamra, R. A. Duine, and P. Yan, Quantum magnonics: When magnon spintronics meets quantum information science, Phys. Rep. **965**, 1 (2022).

[21] B. Flebus, D. Grundler, B. Rana, Y. Otani, I. Barsukov, A. Barman, G. Gubbiotti, P. Landeros, J. Akerman, U. S. Ebels *et al.*, The 2024 magnonics roadmap, J. Phys.: Condens. Matter **36**, 363501 (2024).

[22] S. Zheng, Z. Wang, Y. Wang, F. Sun, Q. He, P. Yan, and H. Y. Yuan, Tutorial: Nonlinear magnonics, J. Appl. Phys. **134**, 151101 (2023).

[23] T. Makiuchi, T. Hioki, H. Shimizu, K. Hoshi, M. Elyasi, K. Yamamoto, N. Yokoi, A. A. Serga, B. Hillebrands, G. E. W. Bauer *et al.*, Persistent magnetic coherence in magnets, Nat. Mater. **23**, 627 (2024).

[24] C. Mathieu, V. T. Synogatch, and C. E. Patton, Brillouin light scattering analysis of three-magnon splitting processes in yttrium iron garnet films, Phys. Rev. B **67**, 104402 (2003).

[25] O. Wojewoda, F. Ligmajer, M. Hrtoň, J. Klíma, M. Dhankhar, K. Davídková, M. Staňo, J. Holobrádek, J. Krčma, J. Zlámal *et al.*, Observing high-k magnons with Mie-resonance-

enhanced Brillouin light scattering, Commun. Phys. **6**, 94 (2023).

[26] L. Körber, K. Schultheiss, T. Hula, R. Verba, J. Fassbender, A. Kákay, and H. Schultheiss, Nonlocal stimulation of three-magnon splitting in a magnetic vortex, Phys. Rev. Lett. **125**, 207203 (2020).

[27] L. Körber, C. Heins, T. Hula, J.-V. Kim, S. Thlang, H. Schultheiss, J. Fassbender, and K. Schultheiss, Pattern recognition in reciprocal space with a magnon-scattering reservoir, Nat. Commun. **14**, 3954 (2023).

[28] C. L. Ordóñez Romero, B. A. Kalinikos, P. Krivosik, W. Tong, P. Kabos, and C. E. Patton, Three-magnon splitting and confluence processes for spin-wave excitations in yttrium iron garnet films: Wave vector selective Brillouin light scattering measurements and analysis, Phys. Rev. B **79**, 144428 (2009).

[29] H. Kurebayashi, O. Dzyapko, V. E. Demidov, D. Fang, A. J. Ferguson, and S. O. Demokritov, Controlled enhancement of spin-current emission by three-magnon splitting, Nat. Mater. **10**, 660 (2011).

[30] H. J. J. Liu, G. A. Riley, C. L. Ordóñez Romero, B. A. Kalinikos, and K. S. Buchanan, Time-resolved study of nonlinear three-magnon processes in yttrium iron garnet films, Phys. Rev. B **99**, 024429 (2019).

[31] H. Schultheiss, X. Janssens, M. van Kampen, F. Ciubotaru, S. J. Hermsdoerfer, B. Obry, A. Laraoui, A. A. Serga, L. Lagae, A. N. Slavin, B. Leven, and B. Hillebrands, Direct current control of three magnon scattering processes in spin-valve nanocontacts, Phys. Rev. Lett. **103**, 157202 (2009).

[32] H. Suhl, The theory of ferromagnetic resonance at high signal powers, J. Phys. Chem. Solids **1**, 209 (1957).

[33] S. O. Demokritov, V. E. Demidov, O. Dzyapko, G. A. Melkov, A. A. Serga, B. Hillebrands, and A. N. Slavin, Bose-Einstein condensation of quasi-equilibrium magnons at room temperature under pumping, Nature (London) **443**, 430 (2006).

[34] A. J. E. Kreil, D. A. Bozhko, H. Yu. Musiienko-Shmarova, V. I. Vasyuchka, V. S. L'vov, A. Pomyalov, B. Hillebrands, and A. A. Serga, From kinetic instability to Bose-Einstein condensation and magnon supercurrents, Phys. Rev. Lett. **121**, 077203 (2018).

[35] M. Schneider, D. Breitbach, R. O. Serha, Q. Wang, A. A. Serga, A. N. Slavin, V. S. Tiberkevich, B. Heinz, B. Lägel, T. Brächer, C. Dubs, S. Knauer, O. V. Dobrovolskiy, P. Pirro, B. Hillebrands, and A. V. Chumak, Control of the Bose-Einstein condensation of magnons by the spin Hall effect, Phys. Rev. Lett. **127**, 237203 (2021).

[36] M. Mohseni, A. Qaiumzadeh, A. A. Serga, A. Brataas, B. Hillebrands, and P. Pirro, Bose-Einstein condensation of quasi-equilibrium magnons at room temperature under pumping, New J. Phys. **22**, 083080 (2020).

[37] J. W. Rao, B. Yao, C. Y. Wang, C. Zhang, T. Yu, and W. Lu, Unveiling a pump-induced magnon mode via its strong interaction with Walker modes, Phys. Rev. Lett. **130**, 046705 (2023).

[38] C. Zhang, J. Rao, C. Y. Wang, Z. J. Chen, K. X. Zhao, B. Yao, X.-G. Xu, and W. Lu, Control of magnon-polariton hybridization with a microwave pump, Phys. Rev. Appl. **20**, 024074 (2023).

[39] C. Wang, J. Rao, Z. Chen, K. Zhao, L. Sun, B. Yao, T. Yu, Y.-P. Wang, and W. Lu, Enhancement of magnonic frequency combs by exceptional points, Nat. Phys. **20**, 1139 (2024).

[40] T. Qu, A. Hamill, R. H. Victora, and P. A. Crowell, Oscillations and confluence in three-magnon scattering of ferromagnetic resonance, Phys. Rev. B **107**, L060401 (2023).

[41] J. Inman, Y. Xiong, R. Bidthanapally, S. Louis, V. Tyberkevych, H. Qu, J. Sklenar, V. Novosad, Y. Li, X. Zhang *et al.*, Hybrid magnonics for short-wavelength spin waves facilitated by a magnetic heterostructure, Phys. Rev. Appl. **17**, 044034 (2022).

[42] I. S. Maksymov and M. Kostylev, Broadband stripline ferromagnetic resonance spectroscopy of ferromagnetic films, multilayers and nanostructures, Phys. E (Amsterdam, Neth.) **69**, 253 (2015).

[43] See Supplemental Material at http://link.aps.org/supplemental/10.1103/PhysRevB.111.L180410 for the detailed theoretical calculations of magnon dispersion and the nonlinear coupling strength.

[44] P. Röschmann and H. Dötsch, Properties of magnetostatic modes in ferrimagnetic spheroids, Phys. Status Solidi B **82**, 11 (1977).

[45] P. C. Fletcher and R. O. Bell, Ferrimagnetic resonance modes in spheres, J. Appl. Phys. **30**, 687 (1959).

[46] R. L. White, Use of magnetostatic modes as a research tool, J. Appl. Phys. **31**, S86 (1960).

[47] L. R. Walker, Magnetostatic modes in ferromagnetic resonance, Phys. Rev. **105**, 390 (1957).

[48] A. Leo, A. G. Monteduro, S. Rizzato, L. Martina, and G. Maruccio, Identification and time-resolved study of ferrimagnetic spin-wave modes in a microwave cavity in the strong-coupling regime, Phys. Rev. B **101**, 014439 (2020).

[49] T. Qu, A. Venugopal, J. M. Etheridge, W. K. Peria, K. Srinivasan, B. J. H. Stadler, P. A. Crowell, and R. H. Victora, Nonlinear magnon scattering mechanism for microwave pumping in magnetic films, IEEE Access **8**, 216960 (2020).